Journal of Coordination Chemistry

ISSN: 0095-8972 (Print) 1029-0389 (Online) Journal homepage: http://www.tandfonline.com/loi/gcoo20

Synthesis, characterization and molecular structures of copper(II) and nickel(II) complexes derived from diacetylmonooxime thiosemicarbazone and diacetylmonooxime S-benzyl dithiocarbazonate

Nahed M.H. Salem, Laila El Sayed, Wolfgang Haase & Magdi F. Iskander

To cite this article: Nahed M.H. Salem, Laila El Sayed, Wolfgang Haase & Magdi F. Iskander (2015) Synthesis, characterization and molecular structures of copper(II) and nickel(II) complexes derived from diacetylmonooxime thiosemicarbazone and diacetylmonooxime S-benzyl dithiocarbazonate, Journal of Coordination Chemistry, 68:12, 2147-2166, DOI: 10.1080/00958972.2015.1037298

To link to this article: http://dx.doi.org/10.1080/00958972.2015.1037298

Accepted author version posted online: 07 Apr 2015.
Published online: 20 May 2015.

Journal of Coordination Chemistry, 2015
Vol. 68, No. 12, 2147–2166, http://dx.doi.org/10.1080/00958972.2015.1037298

Synthesis, characterization and molecular structures of copper(II) and nickel(II) complexes derived from diacetylmonooxime thiosemicarbazone and diacetylmonooxime S-benzyl dithiocarbazonate

NAHED M.H. SALEM†, LAILA EL SAYED†, WOLFGANG HAASE‡ and MAGDI F. ISKANDER*†

†Faculty of Science, Chemistry Department, Alexandria University, P.O. Box 426, Ibrahimia, Alexandria 21321, Egypt
‡Eduard-Zintl-Institute of Inorganic and Physical Chemistry, Darmstadt University of Technology, Petersenstrasse 20, 64287 Darmstadt, Germany

(*Received 14 November 2014; accepted 18 March 2015*)

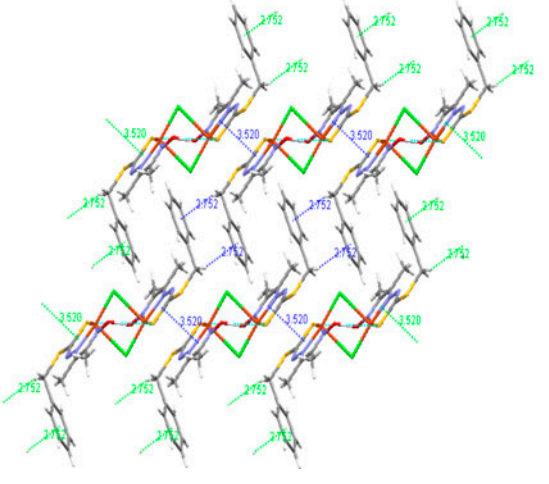

The dinuclear Cu(II) and Ni(II) complexes, [{M(Oxsbz)}$_2$], [{M(Oxtsc)}$_2$] (M = Cu or Ni), [{Cu(HOxsbz)}$_2$](NO$_3$)$_2$, and [{Cu(HOxsbz)Cl}$_2$], as well as the mononuclear [Ni(Oxtsc)HIm] and [Ni(Oxtsc)HPyr], where H_2Oxsbz and H_2Oxtsc refer, respectively, to diacetylmonooxime S-benzyldithiocarbazonate and diacetylmonooxime thiosemicarbazone, have been prepared and characterized by IR, UV–Vis and ^{1}H NMR spectral measurements as well as ESI mass spectra. The magnetic properties of [{Cu(Oxsbz)}$_2$], [{Cu(Oxtsc)}$_2$], [{Cu(HOxsbz)}$_2$](NO$_3$)$_2$, and [{Cu(HOxsbz)Cl}$_2$] have also been studied. The single-crystal diffraction studies indicated that in [{Cu(HOsbz)Cl}$_2$], each Cu(II) is in a distorted square pyramidal environment and the Cu(II) centers are connected by chloride bridges. In both [Ni(Oxtsc)HIm] and [Ni(Oxtsc)HPyr], HIm = imidazole and HPyr = pyrazole, Ni(II) is in a distorted square planar environment, bound to the Oxtsc dianion via

*Corresponding author. Email: m.iskander@link.net

deprotonated oxime nitrogen, imine nitrogen, and deprotonated thiol sulfur; the fourth coordination site is occupied by the heterocyclic nitrogen.

Keywords: Diacetylmonooxime thiosemicarbazone and S-benzyldithiocarbazonate; Copper(II) and nickel(II) complexes; Magnetic properties; X-ray crystal structures

1. Introduction

Diacetylmonooxime has been used as a starting material for the synthesis of NNN [1–4] and NNO [5, 6] tridentate oxime containing Schiff bases, as well as NNO tridentate acyl/aroylhydrazone oximes [7–9]. Condensation of diacetylmonooxime with thiosemicarbazide and S-benzyldithiocarbazide affords the diacetylmonooxime thiosemicarbazone (H_2Oxtsc) (**I**, R=NH_2) [10] and diacetylmonooxime S-benzyldithiocarbazonate (H_2Oxsbz) (**I**, R = S.$CH_2C_6H_5$) [11]. H_2Oxtsc and H_2Oxsbz contain the oxime (C=N–OH) and thioamide (–NH-C=S) moieties. As a ligand, the oxime is potentially ambidentate [12] and can coordinate either through nitrogen [13–16] or oxygen [17]. N-coordination of the oxime leads to an increase in its acidic character, and the formation of the oximate ligand is favored [18]. The oximate can coordinate to one metal ion through nitrogen and to another metal ion through oxygen forming $\mu_{1,2}$ (N,O) oximato-bridged dimers [5, 19–22], homometallic [23–26], or heterometallic [27, 28] polynuclear clusters. Thiosemicarbazone (C=N–NH–C(S)–NH_2) coordinates either in the protonated thione or deprotonated thiolate form [29–32]. There exist examples of metal thiosemicarbazone complexes, in which both protonated thione and deprotonated thiolate forms of the ligand are present in the same complex [33–35]. However, in thiocarbazonate metal complexes, thiocarbazonate (C=N–NH–CSSR) exclusively coordinates in the deprotonated thiolate form [36, 37] (scheme 1).

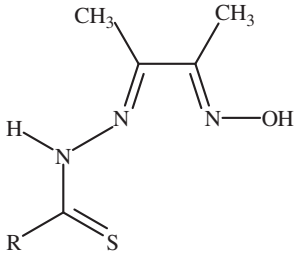

I

R = NH_2 (H_2Oxtsc)

R = $SCH_2C_6H_5$ (H_2Oxsbz)

Scheme 1.

The coordination chemistry of diacetylmonooxime thiosemicarbazone gives both mono- and dinuclear metal(II) complexes [10, 38–43]. Mononuclear metal(III) complexes have also been described [44, 45]. Diacetyl monooxime thiosemicarbazone is a neutral NNS tridentate ligand, and both five-coordinate square pyramidal [Cu(H_2Oxtsc)Cl_2]·H_2O and *mer* octahedral [Ni(H_2Oxtsc)]Cl_2·H_2O complexes [39] have been reported. It can also be a monoanionic NNS tridentate ligand through deprotonation of the thiolimide residue, forming both mononuclear [Pd(HOxtsc)Cl] [42] and dinuclear [{Cu(HOxtsc)Cl}$_2$]·H_2O [10] complexes. In [{Cu(HOxtsc)X}$_2$] complexes, the Cu(II) centers may be bridged by thiolate

sulfur or by the mononegative coligand X [10]. The X-ray crystal structure of [{Cu(HOxtsc)Cl}$_2$] suggests thiolate-bridged dimer. The dinuclear metal(II) complexes [{M(Oxtsc)}$_2$] (M = Ni and Pd) have also been prepared, in which both oxime and thiolimide residues are deprotonated and oximato-bridged dimeric structure has been proposed [43]. Mononuclear metal(III) complexes, [M(HOxtsc)$_2$]X, [M(HOxtsc)(Oxtsc)], and K[M(Oxtsc)$_2$] (M = Fe(III), Co(III), and Rh(III), X = Cl^-, Br^-, NO_3^-, N_3^-, or NCS^-), have also been described [44, 45]. Diacetylmonooxime S-benzyldithiocarbazonate, on the other hand, can be a dianionic NNS tridentate ligand, and the dimeric [{Ni(Oxsbz)}$_2$] complex has been isolated where both oxime and thiolimide residues are deprotonated [11]. The reaction of [{Ni(Oxsbz)}$_2$] with either imidazole (HIm) or pyrazole (HPyr) gave the corresponding mononuclear square planar complexes [Ni(Oxsbz)B] (B = HIm or HPyr) [11]. In the present work, reactions of H_2Oxtsc and H_2Oxsbz with copper(II) and nickel(II) salts have been studied, and the isolated copper(II) and nickel(II) complexes are characterized by elemental analyses, ESI mass spectrometry, FT-IR, UV–vis, and NMR spectroscopic techniques. Variable temperature magnetic susceptibility measurements for copper(II) complexes have also been discussed. The X-ray crystal and molecular structures of [{Cu(HOxsbz)Cl}$_2$], [Ni(Oxtsc)HIm], and [Ni(Oxtsc)HPyr] have been determined.

2. Experimental

2.1. *Materials*

Diacetylmonooxime was obtained from Acros, while pyrazole and imidazole were obtained from Aldrich and used without purification.

2.2. *Preparation of metal free organic ligands*

2.2.1. Preparation of diacetylmonooxime S-benzyldithiocarbazonate (H_2Oxsbz). Diacetylmonooxime S-benzyldithiocarbazonate was prepared as previously described by condensation of diacetylmonooxime with an equimolar amount of S-benzyldithiocarbazate in ethanol [11]. Yield: 75%. M. p. 210 °C. IR (KBr) (cm^{-1}): 3412 ν(OH); 3288 m ν(N–H); 1640 m $\nu(C{=}N)_{hy}$; 1605 m $\nu(C{=}N)_{ox}$.

2.2.2. Preparation of diacetylmonooxime thiosemicarbazone (H_2Oxtsc). Diacetylmonooxime (1.01 g, 0.01 mol) in ethanol (30 mL) and thiosemicarbazide (0.91 g, 0.01 mol) in water (10 mL) were mixed and acidified with a few drops of acetic acid. The resulting mixture was heated under reflux for 3 h, and the white precipitate which separated was removed by filtration, recrystallized from EtOH, and dried under vacuum. Yield: 80%. M.p. 265 °C, Anal. Calcd. for $C_5H_{10}N_4OS$: C, 34.47; H, 5.79; N, 32.18. Found: C, 34.51; H, 5.42; N, 32.11. IR (KBr) (cm^{-1}): 3417s ν(O–H); 3280sh $\nu_{asym}(NH_2)$; 3235s $\nu_{sym}(NH_2)$; 3156s ν(N–H); 1615s $\nu(C{=}N)_{hy}$; 1565 m $\nu(C{=}N)_{ox}$. UV–vis (EtOH, λ_{max}/nm (log ε): 296 (4.45); 245(4.01). ^{1}H NMR (DMSO-d_6, TMS, ppm): 11.59 (1H, oxime OH); 10.20 (1H, CSNH); 8.33 (1H, amine NH); 7.71 (1H, amine NH); 2.05 (3H, s, $CH_3C{=}NN$); 1.95 (3H, s, $CH_3C{=}NO$). EI MS (m/z (RA%), 174 (100), 159 (17.6), 116 (76.4), 98 (15.5), 75 (8.8), 60 (20.3), 42 (39.8).

2.3. *Preparation of Cu(II) complexes*

2.3.1. Preparation of [{CuOxsbz)}$_2$]·H$_2$O (1). To a solution of H_2Oxsbz (0.281 g, 1 mmol) in methanol (40 mL), a solution of copper(II) acetate monohydrate (0.217 g, 1 mmol) in methanol (30 mL) was added dropwise with constant stirring. On refluxing the reaction mixture, with constant stirring, for 3 h, a green precipitate formed. It was filtered while hot, washed with hot methanol (3×5 mL), and dried under vacuum over anhydrous calcium chloride. Yield: 68.0%. Anal. Calcd. for $C_{24}H_{28}N_6O_3S_4Cu_2$ (%): C, 40.95; H, 4.01; N, 11.94. Found: C, 41.33; H, 3.69; N, 11.95. IR (KBr) (cm^{-1}): 1625 m $\nu(C=N)_{hy}$; 1594 m $\nu(C=N)_{ox}$. UV–Vis (saturated solution in DMF, λ_{max}/ nm): 280, 333, 375 sh, 425 sh, 580 b. ESI (+) MS (DMSO) m/z Calcd. (RA): 344.0 (343.9401) (35.38), [(Cu(Oxsbz) + H]$^{1+}$; 366.0 (365.9221) (30.77), [Cu(Oxsbz) + Na]$^{1+}$; 405.0 (404.9894) (35.0), [{Cu (Oxsbz)}$_2$(DMSO)] + 2Na]$^{2+}$; 422.0 (422.0749) (21.54), [Cu(Oxsbz)(DMSO) + H]$^{+}$; 521.3 (522.1915) (20.0), [Cu(Oxsbz)(DMSO)$_2$ + Na]$^{1+}$; 625.4 (625.3421) (12.30), [Cu (HOxsbz)$_2$ + H]$^{1+}$; 687.0 (686.8724) (100.0), [{Cu(Oxsbz)}$_2$] + H]$^{1+}$; 765.0 (765.0072) (13.85), [{Cu(Oxsbz)}$_2$(DMSO) + H]$^{1+}$.

2.3.2. Preparation of [{Cu(Oxtsc)}$_2$]·2H$_2$O (2). This complex was prepared from reaction of $Cu(OAc)_2·H_2O$ with H_2Oxtsc using the same procedure described in Section 2.3.1. Yield: 75.0%. Anal. Calcd. for $C_{10}H_{24}N_8O_6S_2Cu_2$ (%): C, 22.10; H, 4.45; N, 20.61. Found: C, 21.99; H, 4.20; N, 20.24. IR (KBr) (cm^{-1}): 3285s, $\nu_{asym}(NH_2)$; 3220 $\nu_{sym}(NH_2)$; 1592s, $\nu(C=N)_{hy}$; 1510s, $\nu(C=N)_{ox}$. UV–Vis (saturated solution in DMF, λ_{max}/ nm): 275, 333, 425sh, 580 b. ESI (+) MS (DMF) m/z Calcd. (RA): 236.2 (236.7444) (60.23), [Cu(Oxtsc) + H]$^{1+}$; 257.6 (258.7462), (48.07), [Cu(Oxtsc) + Na]$^{1+}$; 308.5 (309.8588) (32.1),[Cu(Oxtsc) DMF + H]$^{1+}$; 382.1 (382.9531) (23.7), [(Cu(Oxtsc)(DMF)$_2$ + H]$^{1+}$; 471.2 (472.5207) (100), [{Cu(Oxtsc)}$_2$ + H]$^{1+}$; 493.8 (494.5027) (20.5), [{Cu(Oxtsc)}$_2$ + Na]$^{1+}$.

2.3.3. Preparation of [{Cu(HOxtsc)}$_2$](NO$_3$)$_2$ (3). A solution of $Cu(NO_3)_2·3H_2O$ (0.24 g, 1.0 mmol) in ethanol (20 mL) was added dropwise with constant stirring to a solution of H_2Oxtsc (0.174 g, 1.0 mmol) in ethanol (30 mL). The reaction mixture was stirred at room temperature for 2 h, and the formed complex was filtered, washed with ethanol, then dried under vacuum. Yield: 66.0%. Anal. Calcd for $C_{10}H_{18}N_{10}O_8S_2Cu_2$ (%): C, 20.10; H, 3.04; N, 23.44. Found: C, 20.41; H, 3.14; N, 22.82. IR (KBr) (cm^{-1}): 3405 m $\nu_{asym}(NH_2)$; 3342s, 3280s, $\nu_{sym}(NH_2)$; 3160s ν(N–H) 1619s $\nu(C=N)_{hy}$; 1555 m $\nu(C=N)_{ox}$; 1385s, 1030s, 826 m, ionic nitrate. Electronic spectrum (saturated solution in DMF, λ_{max}/ nm): 304, 355sh, 425, 600 b. ESI (+) MS (DMSO) m/z Calcd. (RA): 236.2 (236.7644) (66.67), [Cu(Oxtsc) + H]$^{1+}$; 301.2 (299.7771) (3.33), [Cu(HOxtsc)(NO$_3$) + H]$^{1+}$; 412.3 (410.9906) (30.0), [Cu(HOxtsc)$_2$ + H]$^{1+}$; 471.2 (472.5207) (100), [{Cu(Oxtsc)}$_2$ + H]$^{1+}$; 629.9 (628.7904) (3.33), [{Cu(Oxtsc)}$_2$(DMSO)$_2$ + H]$^{1+}$; 708.0 (708.2772) (47.78), [{Cu (Oxtsc)}$_3$ + H]$^{1+}$; 769.9 (770.2821) (2.22), [{Cu(Oxtsc)}$_3$(NO$_3$) + 2H]$^{1+}$; 1004.8 (1007.031) (4.4), [{Cu(Oxtsc)}$_4$NO$_3$ + 2H]$^{1+}$.

2.3.4. Preparation of [{Cu(HOxsbz)Cl}$_2$] (4). A solution of H_2Oxsbz (1.0 mmol, 0.281 g) in ethanol (50 mL) was mixed with a solution of $CuCl_2·2H_2O$ (1.0 mmol, 0.170 g) in ethanol (30 mL). The reaction mixture was heated under reflux, with constant stirring, for 2 h, during which a green precipitate formed. It was collected by filtration, washed with

ethanol, then dried under vacuum. Recrystallization from tetrahydrofuran gave diffraction quality crystals. Yield: 65.0%. Anal. Calcd for $C_{24}H_{28}N_6O_2S_4Cl_2Cu_2$ (%): C, 37.99; H, 3.72; N, 11.07. Found: C, 37.95; H, 3.59; N, 10.92. IR (KBr) (cm^{-1}): 3316s ν(O–H); 1604 m $\nu(C = N)_{hy}$; 1550 m $\nu(C = N)_{ox}$. Electronic spectrum ($CHCl_3$, λ_{max}/nm (logε)): 334 (4.29), 438(3.82), 550sh, 640sh. ESI (+) MS (THF) m/z Calcd. (RA): 417.1 (416.0468) (25.0), $[Cu(Oxsbz)(THF) + H]^{1+}$; 487.1 (488.1533) (100), $[Cu(Oxsbz)(THF)_2 + H]^{1+}$; 500.1 (502.8716) (83.33), $[Cu_2(HOxsbz)_3Cl + 2H]^{2+}$; 986.2 (990.2562) (6.0), $[Cu_2(HOxsbz)_2(Oxsbz) + Na]^{1+}$; 1174.2 (1174.0178) (1.3), $[\{Cu(Oxsbz)\}_3(THF)_2 + H]^{1+}$.

2.4. *Preparation of Ni(II) complexes*

2.4.1. Preparation of [{Ni(Oxsbz)}$_2$] (5). Compound **5** was prepared as previously described [11] from the reaction of H_2Oxsbz with $Ni(OAc)_2{\cdot}4H_2O$ in methanol using (1:1) molar ratio. Anal. Calcd for $C_{24}H_{26}N_6O_2S_4Ni_2$ (%): C, 42.63; H, 3.88; N, 12.34. Found: C, 42.33; H, 3.85; N, 12.46. IR (KBr) (cm^{-1}): $\nu(C = N)_{hy}$ 1600 m; $\nu(C = N)_{ox}$ 1518 m. Electronic spectrum ($CHCl_3$, λ_{max}/nm (logε)): 271(4.16), 314(4.22), 352(4.06), 366sh, 614sh, 660(2.47). ^{1}H NMR (DMSO-d_6, TMS, ppm), 7.10–7.30 (5H, m, aromatic), 4.20 (2H, s, SCH_2), 1.90 (3H, s, $CH_3C = NN$), 1.72 (3H, s, $CH_3C = NO$). FD MS, m/z = 674 (100%).

2.4.2. Preparation of [{Ni(Oxtsc)}$_2$] (6). A solution of $Ni(OAc)_2{\cdot}4H_2O$ (0.281 g, 1.0 mmol) in ethanol (30 mL) was added to a solution of H_2Oxtsc (0.174 g, 1.0 mmol) in ethanol (50 mL). The resulting mixture was treated with a solution of KOH (2.0 mmol) in ethanol (20 mL). On refluxing the reaction mixture with constant stirring for 1 h, a red precipitate formed. It was then filtered, washed with hot ethanol (3 × 5 mL), and dried under vacuum over anhydrous calcium chloride. Yield: 68%; Anal. Calcd for $C_{10}H_{16}N_8O_2S_2Ni_2$ (%):C, 26.01; H, 3.49; N, 24.27. Found: C, 26.05; H, 3.55; N, 23.42. IR (KBr) (cm^{-1}): 3486 m, 3294 m $\nu_{asym}(NH_2)$; 3146s $\nu_{sym}(NH_2)$; 1590 $\nu(C = N)_{hy}$; 1550s $\nu(C = N)_{ox}$. Electronic spectrum (DMF, λ_{max}/nm (logε)): 301(4.26), 354(3.96), 556sh. ^{1}H NMR (DMSO-d_6, TMS, ppm): 7.25 (2H, NH_2), 1.83 (3H, s, $CH_3C = NN$), 1.54 (3H, s, $CH_3C = NO$). ESI (+) MS (DMF) m/z Calcd. (RA): 231.2 (231.9083) (78.3), $[Ni(Oxtsc) + H]^{1+}$; 252.6 (253.8903) (53.8), $[Ni(Oxtsc) + Na]^{1+}$; 304.4 (305.0028) (37.2), $[Ni(Oxtsc)DMF + H]^{1+}$; 378.3 (378.0971) (23.2), $[(Ni(Oxtsc)(DMF)_2 + H]^{1+}$; 462.2 (462.8088) (100), $[\{Ni(Oxtsc)\}_2 + H]^{1+}$; 485.1 (484.7906) (80.3), $[\{Ni(Oxtsc)\}_2 + Na]^{1+}$; 534.7 (535.9030) (18.7), $[\{Ni(Oxtsc)\}_2(DMF) + H]^{1+}$.

2.4.3. Preparation of [Ni(Oxtsc)HIm] (7). To a suspension of dimeric $[\{Ni(Oxtsc)_2\}]$ (0.231 g, 1.0 mmol) in ethanol (50 mL), a sufficient amount of solid imidazole (5.0 mol, 0.34 g) was added and the reaction mixture was heated under reflux until complete dissolution. The reaction mixture was filtered to remove any unreacted starting material, and the filtrate was evaporated to half its volume. On cooling, the imidazole nickel complex separated out, was filtered, washed with diethyl ether (3 × 5 mL), and dried under vacuum. Yield: 59%; Anal. Calcd for $C_8H_{12}N_6OSNi$ (%): C, 32.14; H, 3.44; N, 28.11. Found: C, 32.18; H, 4.04; N, 27.58. IR (KBr) (cm^{-1}): 3438 m $\nu_{asym}(NH_2)$; 3237 m $\nu_{sym}(NH_2)$; 3134 m ν(N–H); 2932 m, 2825w [ν(N–H) + ν(C–H)]; 1637 $\nu(C=N)_{hy}$; 1559s $\nu(C=N)_{ox}$; 1507s, 1450s, 1325 m, 1250 m, 1234 m, 1112 m, 1050 m, 913w. Electronic spectrum (DMF, λ_{max}/nm (logε)): 304(4.12), 348(3.79), 370(3.81), 552sh. ^{1}H NMR (DMSO-d_6, TMS, ppm): 7.87 (1H, NH-imidazole)), 7.15 (3H, imidazole), 6.63 (2H, NH_2), 1.97, 1.84

(3H, s, CH_3C=NN), 1.69, 1.54 (3H, s, CH_3C=NO). ESI (+) MS (DMF/MeOH) m/z Calcd. (RA): 230 (231.9083) (23.13), $[Ni(Oxtsc) + H]^{1+}$; 256.2 (253.8903) (23.88), $[Ni(Oxtsc) + Na]^{1+}$; 326.4 (326.9846) (100), $[Ni(Oxtsc)(DMF) + Na]^{1+}$; 461.0 (462.8088) (23.13), $[\{Ni(Oxtsc)\}_2 + H]^{1+}$; 483.0 (484.7906) (83.58), $[\{Ni(Oxtsc)\}_2 + Na]^{1+}$; 691.0 (693.7091) (5.97), $[\{Ni(Oxtsc)\}_3 + H]^{1+}$; 713.0 (715.5911) (21.64), $[\{Ni(Oxtsc)\}_3 + Na]^{1+}$; 944.9 (946.5915) (32.09), $[\{Ni(Oxtsc)\}_4 + Na]^{1+}$.

2.4.4. Preparation of [Ni(Oxtsc)HPyr] (8). The pyrazole complex [Ni(Oxtsc)HPyr] was prepared from reaction of $[\{Ni(Oxtsc)\}_2]$ with excess pyrazole using the same procedure described for the corresponding imidazole complex. Anal. Calcd for $C_8H_{12}N_6OSNi$ (%): C, 32.14; H, 3.44; N, 28.11. Found: C, 32.32; H, 3.93; N, 27.85. IR (KBr) (cm^{-1}): 3288 m, $\nu_{asym}(NH_2)$ + $\nu_{sym}(NH_2)$; 3163 m ν(N–H); 2863 m, 2838w [ν(N–H)+ν(C–H)]; 1605 $\nu(C = N)_{hy}$; 1559s $\nu(C = N)_{ox}$. Electronic spectrum (DMF, λ_{max}/nm (logε)): 303(4.24), 366 (3.96), 530sh. ^{1}H NMR (DMSO-d_6, TMS, ppm): 7.84 (1H, NH pyrazole), 7.30–6.82 (3H, pyrazole), 6.26 (2H, NH_2), 2.01 (3H, s, CH_3C = NN), 1.95 (3H, s, CH_3C = NO). ESI (+) MS (DMF/MeOH) m/z Calcd. (RA): 230.2 (231.9083) (12.78), $[Ni(Oxtsc) + H]^{1+}$; 256.3 (253.8903) (6.77), $[Ni(Oxtsc) + Na]^{1+}$; 298.3 () (12.78), $[Ni(Oxtsc)(HPyr) + H]^{1+}$; 326.4 (326.9846) (70.68), $[Ni(Oxtsc)(DMF) + Na]^{1+}$; 482.9 (484.7906) (100), $[\{Ni(Oxtsc)\}_2 + Na]^{1+}$; 715.0 (715.5911) (20.30), $[\{Ni(Oxtsc)\}_3 + Na]^{1+}$; 946.9 (946.5915) (39.1), $[\{Ni(Oxtsc)\}_4 + Na]^{1+}$.

2.5. *Physical measurements*

Elemental analyses (C, H, and N) were performed at the Micro analytical Laboratory, Institut für Organische Chemie Technische Universität, Darmstadt, Germany. Infrared spectra were recorded on a Perkin–Elmer 1430 Data system and/or a Perkin–Elmer (FT-IR) Paragon 1000 PC spectrophotometer. Solid samples were examined as KBr disks. The UV–vis absorption spectra were recorded on a V-530 Jasco, recording spectrophotometer, using 10-mm quartz cells and/or a double-beam ratio-recording Lambda 4B Perkin–Elmer spectrophotometer. ^{1}H NMR spectra were recorded on a Bruker WM 300 using tetramethylsilane (TMS) as an internal standard. ESI mass spectra were recorded on an Esquire-LC from Bruker Daltonic Nebulizer 10psi (dry gas 8 L min^{-1}, dry temperature 250 °C). Theoretical isotopic distribution patterns for ionic species were generated using ISOFORM program and/or Sheffield University Chemputer software [46]. Magnetic susceptibilities of powdered dried samples were recorded on a Faraday-type magnetometer using a sensitive computer controlled D-200 Cahn RG microbalance. The magnetic field applied was ~1.5 T [47]. Experimental susceptibility data were corrected for the underlying diamagnetism using Pascal's constants.

X-ray diffraction data for **4**, **7,** and **8** were collected on an Oxford Diffraction Xcalibur (TM) single-crystal X-ray diffractometer with Sapphire CCD detector. Graphite monochromated Mo K_α radiation (λ = 0.71013 Å) was used. The structures were solved by direct methods with SHELXS-97 [48] and refined with full-matrix least squares on F^2 using SHELXL-97 [48]. Hydrogens were positioned with idealized geometry using a riding model and were refined with isotropic displacement parameter. Drawings of the molecules were produced with ORTEP3 [49] or PLATON [50]. Parameters of hydrogen bonds, and other non-covalent bond interactions were measured using PLATON [50] and MERCURY (CCDC) [51]. Crystal data and details concerning data collection and structure refinements for $[\{Cu(HOxsbz)Cl\}_2]$ (**4**), [Ni(Oxtsc)HIm] (**7**), and [Ni(Oxtsc)HPyr] (**8**) are collected in table 1. Selected bond distances and angles for **4** are listed in table 2, while those of **7** and **8** are given in table 3.

3. Results and discussion

3.1. *Synthesis and stoichiometry*

The reaction of H_2Oxsbz and H_2Oxtsc with $Cu(OAc)_2 \cdot H_2O$ in hot methanol using 1:1 M ratio gave, respectively, the neutral dinuclear copper(II) complexes $[\{Cu(Oxsbz)\}_2] \cdot H_2O$ (**1**)

Table 1. Crystal data and structure refinement for $[Cu(Oxsbz)Cl]_2$, [Ni(OxtscHIm)], and [Ni(Oxtsc)HPyr)].

	$[Cu(Oxsbz)Cl]_2$ (**4**)	[Ni(Oxtsc)HIm] (**7**)	[Ni(Oxtsc)HPyr)] (**8**)
Empirical formula	$C_{24}H_{28}Cl_2Cu_2N_6O_2S_4$	$C_8H_{12}N_6NiOS$	$C_8H_{12}N_6NiOS$
Formula weight	758.74	299.01	299.01
Temperature (K)	299(2)	293(2)	299(2)
Wavelength (Å)	0.71073	0.71073	0.71093
Crystal system	Triclinic	Orthorhombic	Monoclinic
Space group	P-1	Pca21	P21/c
Unit cell dimensions			
a (Å)	8.380(1)	19.2800(10)	18.106(4)
b (Å)	8.966(1)	33.228(2)	18.121
c (Å)	11.833(2)	7.4243(5)	7.316(2)
α (°)	104.22(1)	90	90
β (°)	91.50(1)	90	94.45(2)
γ (°)	115.77(1)	90	90
Volume ($Å^3$)	770.30(18)	4756.3(5)	2393.1(10)
Z	1	16	8
Calculated density (Mg/m^3)	1.636	1.670	1.660
Absorption coefficient (mm^{-1})	1.859	1.800	1.789
F(000)	386	2464	1232
Crystal size (mm)	0.40×0.18×1.02	0.40×0.40×0.18	0.52×0.12×0.02
Θ range for data collection (°)	4.16 to 26.37	4.12 to 27.23	4.12 to 25.69
Limiting indices	−7≤h≤10, −11≤k≤10, −14≤l≤14	−24≤h≤23, −42≤k≤40, −9≤1≤8	−22≤h≤21, −22≤k≤22, −6≤1≤8
Reflections collected / unique	5189 / 3099 (Rint = 0.0433)	44,155 / 9881 [R(int) = 0.0695]	14,541 / 4517 [R(int) = 0.1341]
Completeness to θ	26.37 98.3%	27.23 96.5%	25.69 99.5%
Refinement method	Full-matrix least–squares on F^2	Full-matrix least–squares on F^2	Full-matrix least–squares on F^2
Data / restraints / parameters	3099 / 0 / 181	9881 /1 / 604	4517 / 0 / 307
Goodness-of-fit on F^2	1.156	1.026	0.980
Final R indices [I>2σ (I)]	R1 = 0.0796, wR2 = 0.1688	R1 = 0.0460, wR2 = 0.1219	R1 = 0.0795, wR2 = 0.0954
R indices (all data)	R1 = 0.0915, wR2 = 0.1152	R1 = 0.0641, wR2 = 0.1321	R1 = 0.2424, wR2 = 0.1402
Largest diff. peak and hole ($e.A^{-3}$)	0.640 and −0.609	0.950 and −0.406	0.368 and −0.375

Table 2. Selected bond distances (Å) and angles (°) for $[\{Cu(Oxsbz)Cl\}_2]$ (**4**).

Cu1–N3	2.016(5)	N3-Cu1-Cl1	93.10(14)
Cu1–N1	1.955(5)	N3-Cu1-Cl1#	87.03(15)
Cu1–S1	2.2603(17)	N3-Cu1-N1	78.28(19)
Cu1–Cl1	2.2489(15)	N1-Cu1-S1	85.08(14)
Cu1–Cl1#	2.8305(18)	N1-Cu1-C11#	98.67(14)
Cu1…Cu1	3.605	N1-Cu1-Cl1	167.14(15)
		N3-Cu1-S1	163.20(14)
		Cl1-Cu1-Cl1#	90.30(6)
		Cu1-Cl1#-Cu1	98.32(6)

Symmetry transformations used to generate equivalent atoms: #1 −x,−y + 1,−z + 1.

Table 3. Selected bond distances (Å) and angles (°) for [Ni(Oxtsc)HIm] (**7**) and [Ni(Oxtsc)HPyr] (**8**).

[Ni(Oxtsc)HIm] (**7**)							
Ni1–mol. unit		Ni2–mol. unit		Ni3-mol. unit		Ni4-mol. unit	
Ni1–N1	1.903(8)	Ni2–N7	1.905(9)	Ni3-N13	1.902(9)	Ni4–N19	1.913(7)
Ni1–N2	1.848(7)	Ni2–N8	1.909(6)	Ni3–N14	1.784(7)	Ni4–N20	1.863(8)
Ni1–S1	2.156(3)	Ni2–S2	2.175(2)	Ni3–S3	2.160(2)	Ni4–S4	2.164(3)
Ni1–N4	1.924(9)	Ni2–N10	1.927(6)	Ni3–N16	1.860(7)	Ni4–N22	1.876(8)
N1–Ni1–N4	100.2(4)	N7–Ni2–N10	97.9(3)	N13–Ni3–N16	96.0(3)	N19–Ni4–N22	96.9(3)
N2–Ni1–N1	81.5(3)	N8–Ni2–N7	83.9(3)	N14–Ni3–N13	83.0(3)	N20–Ni4–N19	84.6(3)
N4–Ni1–S1	92.0(3)	N10–Ni2–S2	92.9(2)	N16–Ni3–S4	93.0(2)	N22–Ni4–S4	92.5(3)
N2–Ni1–S1	86.3(2)	N8–Ni2–S2	85.2(2)	N14–N3–S3	87.9(2)	N20–Ni4–S4	86.0(3)
N1–Ni1–S1	167.5(3)	N7–Ni2–S2	169.1(2)	N13–Ni3–S3	170.82(19)	N19–Ni4–S4	170.5(2)
N2–Ni1–N4	178.1(4)	N8–Ni2–N10	177.2(4)	N14–Ni3–N16	177.2(4)	N20–Ni4–N22	177.3(4)
[Ni(Oxtsc)HPyr] (**8**)							
Ni1–mol. unit		Ni2-mol. unit					
Ni1–N1	1.893(8)	Ni2–N7	1.829(7)				
Ni1–N2	1.847(7)	Ni2–N8	1.983(7)				
Ni1–S1	2.150(3)	Ni2–S2	2.041(3)				
Ni1–N4	1.854(8)	Ni2–N10	2.019(8)				
N1–Ni1–N4	97.6(4)	N7–Ni2–N10	100.2(4)				
N2–Ni1–N1	82.7(4)	N7–Ni2–N8	79.9(4)				
N4–Ni1–S1	93.0(3)	N10–Ni2–S2	92.2(3)				
N2–Ni1–S1	86.7(3)	N8–Ni2–S2	87.7(2)				
N1–Ni1–S1	169.4(3)	N7–Ni2–S2	167.5(3)				
N2–Ni1–N4	179.6(4)	N8–Ni2–N10	179.5(3)				

(**II**, M = Cu, R = S·$CH_2C_6H_5$) and [{Cu(Oxtsc)}$_2$]·$2H_2O$ (**2**) (**II**, M = Cu, R = NH_2). The same reaction with $Ni(OAc)_2·4H_2O$ in ethanol also afforded the dinuclear [{Ni(Oxsbz)}$_2$] (**5**) (**II**, M = Ni, R = S·$CH_2C_6H_5$) and [{Ni(Oxtsc)}$_2$] (**6**) (**II**, M = Ni, R = NH_2) complexes, respectively. The reaction of H_2Oxsbz with an equivalent amount of $Cu(NO_3)_2·3H_2O$ in hot methanol proceeded with deprotonation of both oxime and thiolimide and eventually gave the neutral dinuclear [{Cu(Oxsbz)}$_2$]·H_2O (**1**) (**II**, M = Cu, R = S.$CH_2C_6H_5$) similar to that obtained from the reaction with $Cu(OAc)_2·H_2O$. However the reaction of H_2Oxtsc with $Cu(NO_3)_2·3H_2O$ gave the dimeric nitrate complex [{Cu(HOxtsc)}$_2$]$(NO_3)_2$ (**3**) (**III,** M = Cu, R = NH_2). Different from the reaction of $CuCl_2·2H_2O$ with H_2Oxtsc which was reported to give the monomeric [Cu(H_2Oxtsc)Cl_2]·H_2O [39], the reaction of $CuCl_2·2H_2O$ with H_2Oxsbz proceeded with the formation of the dinuclear [{Cu(HOxsbz)Cl}$_2$] (**4**) (scheme 2).

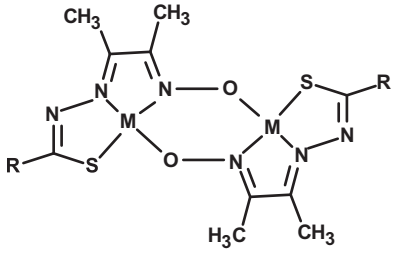

II

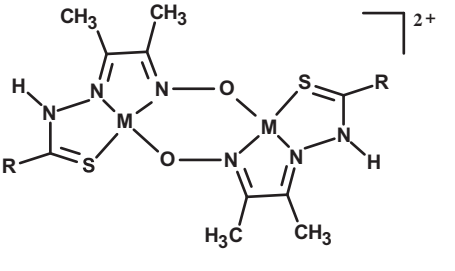

III

Scheme 2.

The ternary Ni(II) complexes [Ni(Oxsbz)HIm] and [Ni(Oxsbz)HPyr] have been previously prepared from reaction of the neutral dimer [{Ni(Oxsbz)}$_2$] with excess (5-10 equivalents) imidazole (HIm) or pyrazole (HPyr) [11]. In this work, both [Ni(Oxtsc)HIm] (**7**) and [Ni(Oxtsc)HPyr] (**8**) have been similarly prepared from the reaction [{Ni(Oxtsc)}$_2$] with five equivalents of imidazole or pyrazole, respectively. Attempts to prepare the ternary Cu (II) complexes [Cu(Oxsbz)B] and [Cu(Oxtsc)B] (B = HIm and HPyr) by reacting the corresponding dinuclear [{Cu(Oxsbz)}$_2$] and [{Cu(Oxtsc)}$_2$] with excess imidazole or pyrazole were unsuccessful, and the starting dinuclear dimers were recovered. Similarly, the reaction of H_2Oxsbz and H_2Oxtsc with $Cu(OAc)_2{\cdot}H_2O$ in the presence of excess imidazole or pyrazole failed to give the expected ternary Cu(II) complex but proceeded with formation of the neutral dinuclear [{Cu(Oxsbz)}$_2$] and [{Cu(Oxtsc)}$_2$] complexes. This behavior implies that neither imidazole nor pyrazole can rupture the oximate bridges in [{Cu(Oxsbz)}$_2$] or [{Cu (Oxtsc)}$_2$].

3.2. *Infrared and mass spectra*

The IR and (+) ESI mass spectral data for H_2Oxsbz and H_2Oxtsc as well as their Cu(II) and Ni(II) complexes are given in the Experimental section. The IR spectra of Cu(II) (**1** and **2**) and Ni(II) (**5** and **6**) complexes lack absorptions which could be attributed to oxime ν(OH) and thione amide ν(NH). The $\nu(C=N)_{hy}$ and $\nu(C=N)_{ox}$ of the diimine residue in the spectra of Cu(II) and Ni(II) complexes appear at lower frequencies as compared to those of H_2Oxsbz and H_2Oxtsc, respectively. The stoichiometry and the IR spectral data recorded for **1**, **2**, **5,** and **6** suggest deprotonation of both oxime and thiohydrazone residues and a dimeric structure with two oximate bridges (**II**, M = Cu or Ni and R = NH_2 or $CH_2C_6H_5$) for these complexes. Their (+) ESI mass spectra display base peaks of 100% relative intensity corresponding to either dimeric monoprotonated and/or solvated dinuclear cations, confirming the dimeric nature of these complexes. The spectra also show peaks corresponding to the protonated mononuclear cations originating from rupture of the oximate bridges. Deprotonation of the mononuclear cations followed by self-assembly leads to tri- and tetranuclear species.

The IR spectrum of [{Cu(HOxtsc)}$_2$]$(NO_3)_2$ (**3**) shows an intense absorption at 3160 cm^{-1} due to thioamide ν(N–H), implying that the thiosemicarbazone oxime in **3** is a mononegative NNS tridentate ligand where the oxime residue is deprotonated while the thiosemicarbazone remains in the thioamide [-NH-(C = S)] form. Deprotonation of the oxime leads to formation of the dimeric structure (**III**, M = Cu, R = NH_2), where the two Cu(II) are linked by oximate bridges. The presence of a base peak at m/z = 471.2, in the (+) ESI mass spectrum of **3**, corresponding to the protonated dinuclear cation [{Cu (Oxtsc)}$_2$ + H]$^{1+}$ is in agreement with the dinuclear structure of the Cu(II) complex. Moreover, the presence of ionic nitrate is revealed by intense bands at 1384, 1030, and 824 cm^{-1} in the IR spectrum of this complex [52].

No absorption due to the thione amide ν(N–H) has been observed in the IR spectrum of [{Cu(HOxsbz)Cl}$_2$] (**4**). The spectrum, however, displays a strong absorption at 3316 cm^{-1} due to oxime hydrogen-bonded ν(OH). This indicates that the carbodithioate oxime in **4** is coordinated to Cu(II) via oxime nitrogen, imine nitrogen, and deprotonated thiolimide sulfur. The X-ray crystal structure of [{Cu(HOxsbz)Cl}$_2$] (Section 3.5.1) reveals a dinuclear structure where the two Cu(II) ions are linked through two chloride bridges. Although the dimeric nature of **4** has been confirmed by X-ray crystal structure, the (+) ESI mass

spectrum in THF shows the base peak at m/z = 487.1 corresponding to the mononuclear solvated cation $[Cu(Oxsbz)(THF)_2 + H]^{1+}$, due to rupture of the chloride bridges in the coordinating THF solvent.

3.3. *Electronic spectra*

The solution electronic spectra of **1**, **2,** and **3** in DMF are similar and show absorptions from 330 to 380 nm attributable to different intraligand (L–L*) transitions. The spectra also show absorption at *ca.* 425 nm which can be attributed to LMCT (S→Cu) transition from the S donor to Cu(II) [53–55]. The d–d spectra appear as a broad absorption at 570–600 nm due to the energetically close $^2B_{1g} \rightarrow {}^2A_{1g}$, $^2B_{2g}$, and ^2E_g electronic transitions of Cu(II) in a square planar environment [56]. The electronic spectrum of **4** in $CHCl_3$ shows L–L* intraligand absorptions at 334 and 360 sh nm, while the LMCT (S→Cu) absorption is at 435 nm [53–56]. The d–d absorption bands at 550 nm with a well-defined shoulder at 640 nm are consistent with a square pyramidal geometry [56].

3.4. *Molecular structures and self–assembly*

3.4.1. [{Cu(HOxsbz)Cl}$_2$] (4). The structure of **4**, figure 1, consists of a discrete dicopper (II) molecular unit, in which the two copper(II) ions are bridged by two chlorides. The coordination geometry around copper(II) is best described as distorted square pyramidal as evident from the magnitude of the trigonality index ($\tau = 0.067$) [$\tau = \beta–\alpha / 60$, α = N3–Cu1–S1 = 163.20, β = N1-Cu1–Cl1 = 167.14; for perfect square pyramidal $\tau = 0$, while for trigonal bipyramid $\tau = 1$] [57]. The four basal positions are occupied by oxime N3 (Cu1–N3 = 2.015(4) Å), hydrazone N1 (Cu1–N1 = 1.957(4) Å), and the deprotonated thiolamide S1 (Cu1–S1 = 2.259(16) Å) of the mononegative NNS tridentate hydrazone oxime ligand. The fourth equatorial coordination site is occupied by one of the two chlorides (Cu1–Cl1 = 2.248(14) Å), while the apical fifth coordination site is occupied by the other chloride (Cu1–Cl1 = 2.831(17) Å).

The four equatorial donors around copper(II) are nearly coplanar, with the Cu1 displaced by 0.100 Å from the mean basal plane toward the apical Cl1. The two chlorides in the Cu_2Cl_2 plane make a four-membered ring where the Cu1–Cl1–Cu1 and Cl1–Cu1–Cl1 angles are 89.68° and 90.32°, respectively, while the Cu–Cu distance is 3.606 Å. The Cu_2Cl_2 plane is nearly planar and makes an angle of 85.00° with the basal mean plane (N1, N3, Cu1, S1, Cl1).

The oxime O1H1 proton of one Cu(HOxsbz)Cl is involved in intramolecular hydrogen bond formation with the thiolimide S1 of the other Cu(HOxsbz)Cl unit [O1H1···S1, O1···S1 = 3.413 Å] giving a seven-membered ring of graph set $\mathbf{R}_1^1$**(7)** [58]. The dimeric units are interconnected by two reciprocal intermolecular CH–π interactions [59] between the acidic methylene C4H4A proton and the π_1–system of the phenyl ring (C5–C10) of the adjacent dimeric unit (C4H4A···C_g1 = 2.752 Å, C7–C_g1–H4A = 98.56° and C10–C_g1–H4A = 81.06°). These CH–π interactions lead to formation of a chain of dimers propagating along the *c*-axis. In the basal plane, the two five-membered chelate rings with delocalized π–system can behave as aromatic rings [60] and be involved in π–π interactions. Consequently, the dimers are connected via two reciprocal π–π interactions between the diimine (N1C2C3N3Cu1) (Cg2) chelate ring and the hydrazone (N1N2C1S1Cu1) (Cg3) chelate ring of the adjacent dimer [Cg2–Cg3 = 3.520 Å, forming a 1–D assembly along the *a*-axis. In

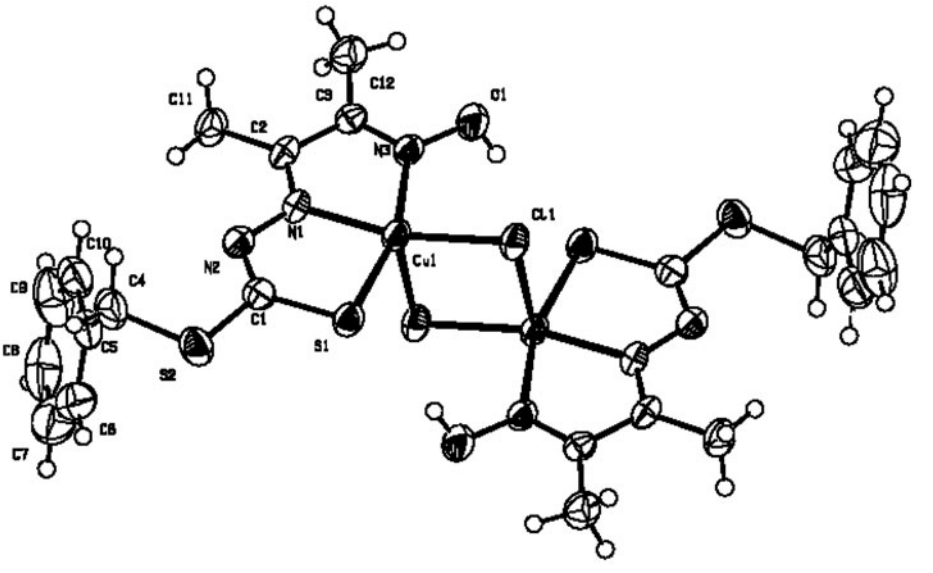

Figure 1. ORTEP representation of [{Cu(HOxsbz)Cl}$_2$] (**4**) with atom labeling scheme; displacement ellipsoids are drawn at 50% probability level.

this assembly, the π–π stacking between chelate rings results in an alternating short intramolecular Cu–Cu separation (3.605 Å) within the Cu_2Cl_2 bridge and a long intermoleclar Cu–Cu distance (4.782 Å) between the basal planes. Both CH–π interactions along the *c*-axis and π–π interactions along *a*-axis give the two-dimensional sheet extended parallel to the *ac*-plane.

3.4.2. [Ni(Oxtsc)HIm] (7). The crystal structure of **7**, figure 2, consists of four crystallographically independent molecular units, Ni1-, Ni2-, Ni3-, and Ni4- molecular units. In these molecular units, the central Ni(II) is in a distorted square planar environment, bound to the thiosemicarbazone oxime via deprotonated oxime nitrogen, imine nitrogen, and deprotonated thiol sulfur forming 5,5–bicyclic chelate rings. The fourth coordination site is occupied by the imidazole nitrogen. The average bond distances between Ni(II) and oxime nitrogen (N1, N7, N13, and N19) (1.906 Å), imine nitrogen (N2, N8, N14, and N20) (1.851 Å), deprotonated thiol sulfur (S1, S2, S3, and S4), (2.164 Å), and imidazole nitrogen (N4, N10, N16, and N22) (1.897 Å), table 3, are within the normal range for similar square planar Ni(II) complexes derived from dianionic NNS tridentate thiosemicarbazones and dithiocarbazates [11]. Deviation from idealized square planar arrangement in **7** is evident from the values, table 3, of both *cis* and *trans* bond angles around the central Ni(II). In Ni1−, Ni2−, Ni3−, and Ni4 mol units, the imidazole plane is not coplanar with the corresponding Ni(II) coordination plane but makes angles of 32.69°, 51.80°, 50.79°, and 36.33°, respectively.

The Ni1 mol. units are interconnected via (N6H62···N3, N6···N3 = 3.518(12) Å) hydrogen bonds between the aminic N6H62 proton and hydrazinic N3 nitrogen (open chain aminic–hydrazinic interactions, figure 3, table 4, forming a one-dimensional **C(4)** chain [58] (Ni1-chain) extending parallel to the *c*-axis. In this chain, the Ni1 units are arranged in

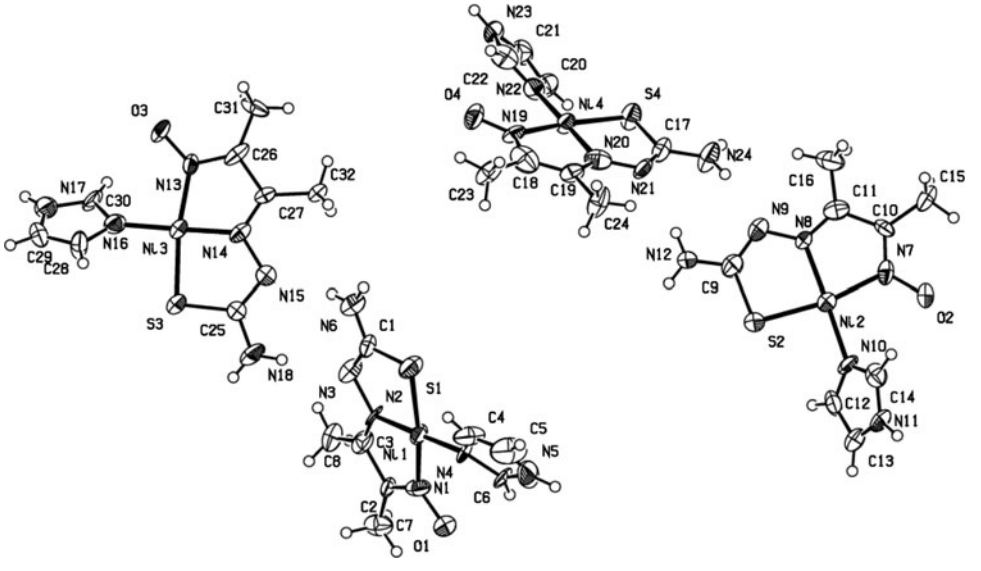

Figure 2. ORTEP representation of [Ni(Oxtsc)HIm] (**7**) with atom labeling scheme; displacement ellipsoids are drawn at 50% probability level.

horizontal–vertical fashion where the angle between the successive Ni1 coordination planes (N1, N2, S1, Ni1, N4) is 79.76°. The Ni1 units of Ni1 chain are linked to adjacent Ni2 units through imidazole–oximate interactions, figure 4, table 4, where the imidazole N5H51 proton of Ni1 unit is involved in hydrogen bond formation with the oximate O2 of adjacent Ni2 unit (N5H51···O2, N5···O2 = 2.853(13) Å), while the imidazole N11H111 proton of this Ni2 unit forms a (N11H111···O1, N11···O1 = 2.736(13) Å) hydrogen bond with oxime O1 of the next parallel Ni1 unit in the same Ni1-chain. These imidazole–oximate interactions give a **C(8)** [58] Ni1-Ni2 chain. The formed chains are further linked through two pairs of reciprocal (N12H122···O1, N12···O1 = 2.886(8) Å) hydrogen bonds between the oximate O1 oxygens of Ni1 units and the aminic N12H122 protons of the Ni2 units of the

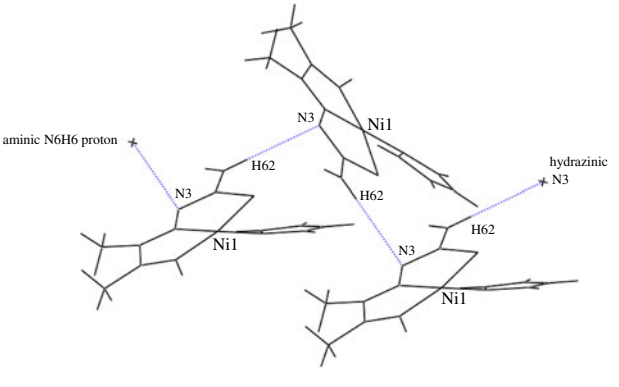

Figure 3. Diagrammatic representation of the open chain aminic–hydrazinic hydrogen bonding in [Ni(Oxtsc)HIm] (**7**).

Table 4. Non-covalent bond interactions in [Ni(Oxtsc)HIm] (**7**).

D–H···A	Symmetry code	D–H (Å)	H···A (Å)	D···A (Å)	D–H···A (°)
Open chain aminic–hydrazinic interactions					
Ni1- chain formation					
N62H62···N3	−½–x, y, −½+z	0.859	2.742	3.518(12)	151.04
Ni4- chain formation					
N24H242···N21	½–x, y, −½+z	0.861	2.808	3.556(12)	146.19
Imidazole–oximate interactions					
Ni1-Ni2 chain formation					
N11H111···O1	x, y, 1+z	0.860	1.88	2.736(13)	175.0
N5H51···O2	x, y, 1+z	0.860	2.12	2.853(13)	143.0
Ni4-Ni3 chain formation					
N17H171···O4	½–x, y, −½+z	0.860	1.86	2.705(12)	168.0
N23H231···O3	½+x, −1–y, 1+z	0.860	2.13	2.820(11)	137.0
Aminic–oximate interactions					
^{2}D Ni1-Ni2 layer formation					
N12H122···O1	−½+x, −1–y, −1+z	0.860	2.10	2.886(8)	153.0
^{2}D Ni4-Ni3 layer formation					
N18H182···O4	x, y, −1+x	0.8660	2.16	2.936(10)	149.0
Cyclic aminic–hydrazinic interactions					
^{3}D framework formation					
N6H61···N15	x, y, 1+z	0.860	2.31	3.161(11)	168.0
N18H181···N3	x, y, −1+z	0.860	2.07	2.918(10)	169.0
N24H241···N9	½–x, −1+y, −1.5+z	0.860	2.29	3.141(12)	169.0
N12H121···N21	−x, −1–y, −1.5+z	0.860	2.14	2.999(9)	174.0

symmetry inverted adjacent chain, thus giving two-dimensional layer of Ni1–N2 chains extending parallel to the *ac*-plane (Ni1–Ni2 layer).

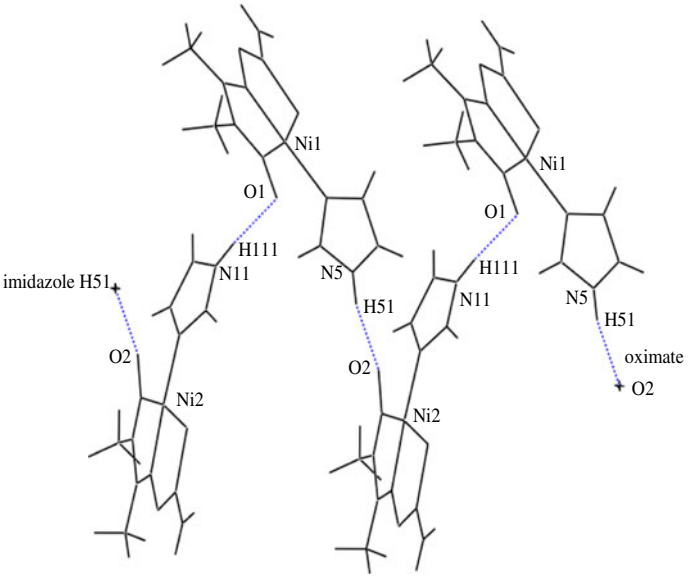

Figure 4. Diagrammatic representation of the imidazole–oximate hydrogen bonding in [Ni(Oxtsc)HIm] (**7**).

Similarly the Ni4 units are also interconnected via (N24H242···N21, N24···N21 = 3.556 (12) Å) hydrogen bonds between the aminic N24H242 proton of Ni4 unit and the hydrazinic N21 of the adjacent unit, forming a one-dimensional **C(4)** [58] Ni4-chain propagating parallel to the *c*-axis. In this Ni4-chain, the angle between successive Ni4 coordination planes (N19, N20, S4, Ni4, N22) is 81.25°. Here again, each Ni4 unit of the Ni4-chain is joined to Ni3 unit through a (N23H231···O3, N23···O3 = 2.820(11) Å) hydrogen bond (imidazole–oximate interactions) while the imidazole N17H171 proton of the Ni3 unit is involved in hydrogen bond formation with the oximate O4 of the adjacent Ni4 unit (N17H171···O4, N17···O4 = 2.705(12) Å), forming a one-dimensional **C(8)** [58] interwoven Ni4–Ni3 chain running parallel to the *c*-axis. The Ni4-Ni3 chains are further linked via two reciprocal pairs of (N18H181···O4, N18···O4 = 2.936(10) Å) hydrogen bonds between the aminic H182 protons of the Ni3 units and oxime O4 oxygens of Ni4 units, giving two-dimensional layer of Ni4–Ni3 chains extending parallel to the *ac*-plane (Ni4–Ni3 layer).

The Ni1 units of Ni1-Ni2 chains in Ni1-Ni2 layer and the Ni3 units of Ni4-Ni3 chains in Ni4-Ni3 layer are paired through (N18H181···N3, N18···N3 = 2.918(10) Å) and (N6H61···N15, N6···N15 = 3.161(11) Å) hydrogen bonds (cyclic aminic–hydrazinic interactions, figure 5, table 4, to form an 8-membered hydrogen-bonded ring [$\mathbf{R_2^2(8)}$] [58]. Similarly, the Ni4 units of Ni4-Ni3 chains in the Ni4-Ni3 layer and Ni2 units of Ni1-Ni2 chains in the Ni1-Ni2 layer are also linked by $\mathbf{R_2^2(8)}$ hydrogen-bonded rings generated by (N12H121···N21, N12···N21 = 2.999(9) Å) and (N24H241···N9, N24···N9 = 3.141(12) Å) hydrogen bond motifs. The interconnection between Ni1-Ni2 and Ni4-Ni3 layers through cyclic aminic–hydrazinic interactions, figure 5, leads to a three-dimensional framework.

3.4.3. [Ni(Oxtsc)HPyr] (8). The crystal structure of **8**, figure 6, consists of two crystallographically independent molecular units, Ni1 and Ni2 units. Selected bond distances and bond angles for both Ni1 and Ni2 units are listed in table 3. In both units, the Ni(II) is in a distorted square planar environment. In the Ni1 unit, the pyrazole plane (C4, C5, C6, N5, N4) is almost coplanar with the corresponding Ni1 coordination plane (N1, N2, S1, N4, Ni1) (dihedral angle = 2.15°), while the angle between the Ni2 coordination plane (N7, N8, S2, N10, Ni2) and the pyrazole plane (C12, C13, C14, N11, N10) is 7.36°.

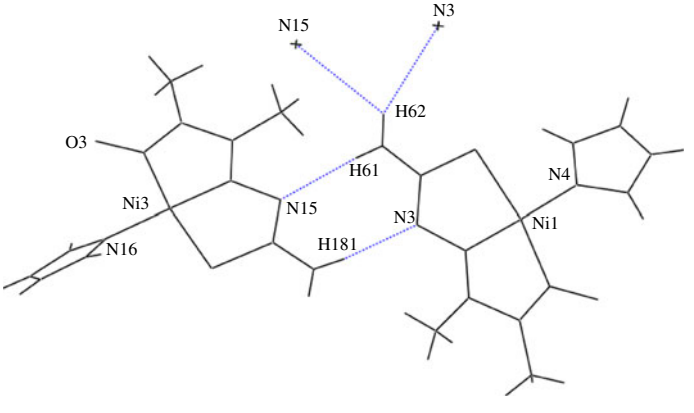

Figure 5. Diagrammatic representation of the cyclic aminic–hydrazinic hydrogen bonding in [Ni(Oxtsc)HIm] (**7**).

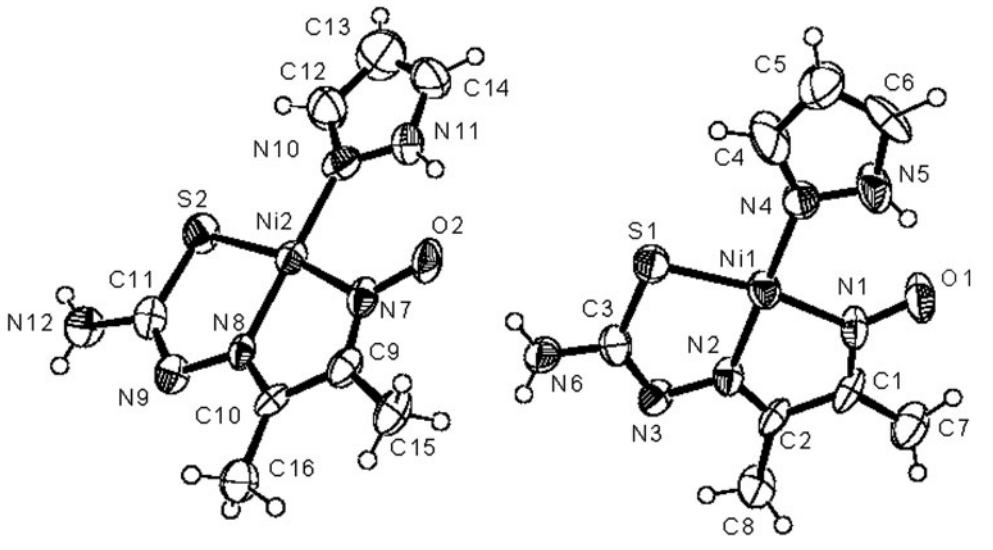

Figure 6. ORTEP representation of [Ni(Oxtsc)HPyr} (**8**) with atom labeling scheme; displacement ellipsoids are drawn at 50% probability level.

In both Ni1 and Ni2 units, the pyrazole N5H5 and N11H11 protons are involved in intramolecular hydrogen bonds (N5H5···O1, N5···O1 = 2.496 Å) and (N11H11···O2, N11···O2 = 2.616 Å) with the corresponding oximate O1 and O2 (table 5). In the crystal lattice of **8**, the adjacent Ni2 units are held together by (N12H122···N9, N12···N9 = 3.266 (10) Å) hydrogen bonds between the aminic N12H122 proton of one unit and the hydrazinic N9 of the adjacent Ni2 unit (open chain aminic–hydrazinic interaction), table 5, forming a one-dimensional **C4** chain [58] running parallel to the *c*-axis (Ni2-chain). The Ni2–chain is further stabilized by (N12H122···N12, N12···N12 = 3.718 Å) and CH–π interactions between the methyl C15H15B proton and the π-system of the pyrazole ring

Table 5. Non-covalent bond interactions in [Ni(Oxtsc)HPyr] (**8**).

D–H···A	Symmetry code	D–H (Å)	H···A (Å)	D···A (Å)	D–H–A (°)
Intramolecular hydrogen bonds					
N5H5···O1	x, y, z	0.860	1.753	2.496(11)	143.21
N11H11···O2	x, y, z	0.860	1.922	2.616(11)	136.66
Intermolecular hydrogen bonds					
Ni2 – chain formation					
N12H122···N9	x, 1.5–y, −½+z x, y, −1+z	0.860	2.502	3.266(10)	148.50
N12H122···N12	x, 1.5–y, −½+z x, y, −1+z	0.860	2.967	3.718	142.12
C15H15B···Cg		0.961	2.727	3.644	159.9
Ni1–Ni2 chain formation					
N12H121···N3	−x, 1–y, 1–z	0.860	2.458	3.317(10)	177.04
N6H62···N9	−x, 1–y, 1–z	0.861	2.204	3.048(10)	166.43
^{2}D layer formation					
N6H62···O2	x, y, z	0.859	2.058	2.899(9)	165.88

(C15H15B···Cg = 2.727 Å), table 5. In this chain, each Ni2 unit is linked to a Ni1 unit through two hydrogen bonds: (i) (N12H121···N3, N12···N3 = 3.317(10) Å) between the aminic N12H121 proton of Ni2 unit and the hydrazinic N3 nitrogen of the adjacent Ni1 unit and (ii) (N6H61···N9, N6···N9 = 3.048(10) Å) between the aminic N6H61 proton of the Ni1 unit and hydrazinic N9 nitrogen of the adjacent Ni2 unit, giving a $\mathbf{R}_2^2$**(8)** [58] eight-membered hydrogen-bonded ring between Ni1 and Ni2 units (cyclic aminic–hydrazinic interactions). These non-covalent bond interactions lead to a tubular Ni1-Ni2 chain propagating parallel to the *c*-axis. The formed chains are further interconnected through two pairs of reciprocal (N6H62···O2, N6···O2 = 2.899(9) Å) hydrogen bonds between aminic N6H62 proton and oximate O2 oxygen, giving a two-dimensional layer of Ni1–Ni2 chains extending parallel to the *bc*-plane.

3.5. *Magnetic measurements*

At room temperature (298 K), the neutral [{Cu(Oxsbz)}$_2$] (**1**) and [{Cu(Oxtsc)}$_2$] (**2**), as well as the cationic nitrate complex [{Cu(HOxtsc)}$_2$](NO$_3$)$_2$ (**3**), show subnormal magnetic moments of 0.96, 1.07, and 0.86 μ_B, respectively, indicating antiferromagnetic coupling between the Cu(II) centers, consistent with a dimeric structure [61]. Variable temperature (4–300 K) magnetic susceptibility measurements recorded for **1**, **2,** and **3** were fitted to the revised Bleaney–Bowers equation [62] (equation 1) using isotropic (Heisenberg) (H = −2JS$_1$. S$_2$) for two interacting S = ½ centers,

$$\chi_m = (1-\rho)\frac{2N_L\mu_{\beta^2}g^2\exp(2J/kT)}{k(T-\theta[(1+3\exp(2J/kT)]} + \rho\frac{2N_L\mu_{\beta^2}g^2}{4kT} + 2N_\alpha \quad (1)$$

where χ_m is expressed per two Cu(II) ions, N_α is the temperature-independent paramagnetism [60 × 10^{-6} cm^3 mol^{-1} per Cu(II)], ρ is the fraction of monomeric impurity, and θ is a correction term for interdimer interactions. A nonlinear regression analysis was carried out, and the best fit magnetic parameters (−2 J, g, ρ, and θ) are listed in table 6. The variation of molar magnetic susceptibility, χ_m, and magnetic moment, μ_{eff}, as a function of temperature for **1** are shown in figure 7. Similar behavior has been recorded for **2** and **3**. The −2 J values estimated for these complexes, table 6, are within the range reported for other oximate-bridged dicopper(II) complexes [1–4, 8, 9, 19, 20] and the dinuclear structure (**II**, M = Cu and R = CH$_2$C$_6$H$_5$ or NH$_2$) can be proposed for **1** and **2**. Similarly, structure (**III**, M = Cu and R = NH$_2$) can be adopted for **3**.

The room-temperature magnetic moment (per Cu(II)) recorded for the dinuclear [{Cu(HOxsbz)Cl}$_2$] (**4**) [1.85 μ_B (298)] is within the normal range reported for magnetically diluted Cu(II) complexes [61]. However, fitting the values of the magnetic susceptibilities

Table 6. The best fit magnetic parameters for Cu(II) complexes derived from diacetylmonooxime thiosemicarbazone and diacetylmonooxime S-benzyldithiocarbazonate.

Complex	μ_{eff} (μ_B) (297)	−2 J (cm^{-1})	*g*	*θ* (K)	*ρ* (%)
[{Cu(Oxsbz)}$_2$]·H$_2$O	0.96	687.0	2.08	0.66	1.20
[{Cu(Oxtsc)}$_2$]·2H$_2$O	1.07	670.0	2.08	0.34	1.96
[{Cu(HOxtsc)}$_2$](NO$_3$)$_2$	0.86	652.0	2.08	2.14	2.60
[{Cu(HOxsbz)Cl}$_2$]	1.85	6.5	2.08	2.53	1.13

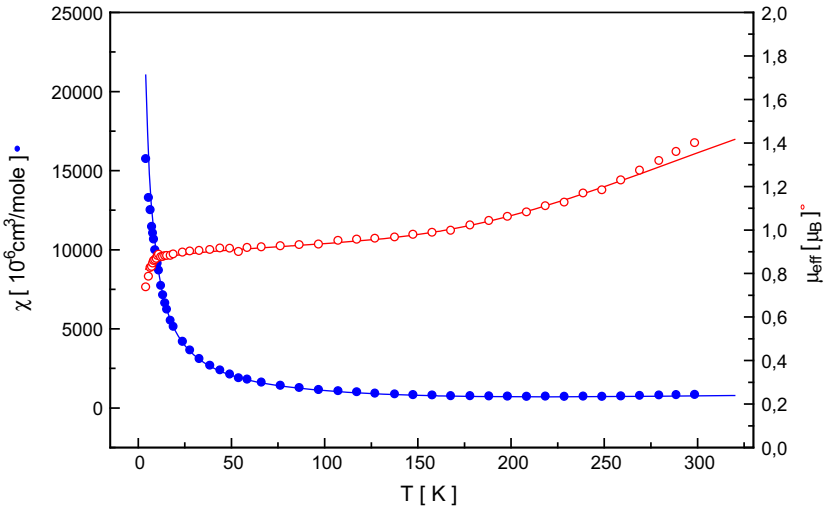

Figure 7. Magnetic susceptibilities χ_M (•) and magnetic moments μ_{eff} (o) *vs* temperature for [{Cu(Oxsbz)}$_2$]·H_2O (**1**). Solid lines represent the best least squares fit to Bleany–Bowers equation with $-2J = 687.0$ cm^{-1}, $\theta = -0.66$, g = 2.08, and $\rho = 1.20$ (%).

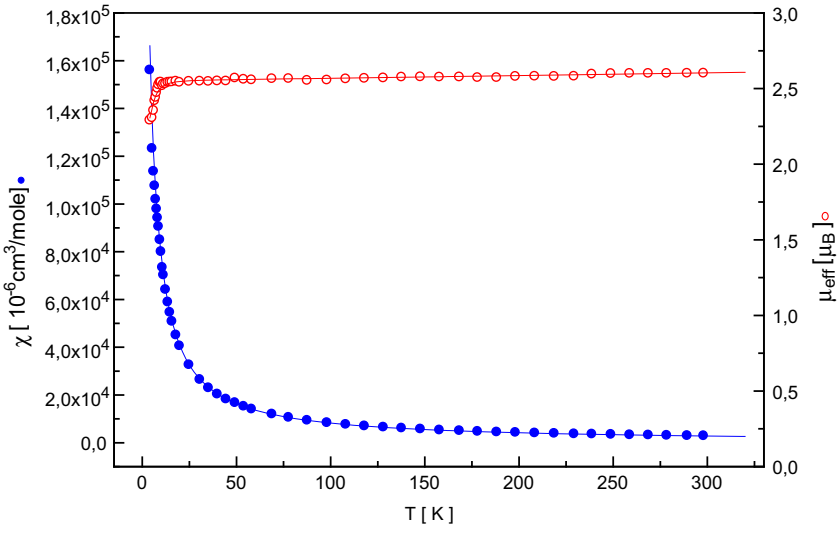

Figure 8. Magnetic susceptibilities χ_M (•) and magnetic moments μ_{eff} (o) *vs* temperature for [{Cu(HOxsbz)Cl}$_2$] (**4**). Solid lines represent the best least squares fit to Bleany–Bowers equation with $-2J = 6.5$ cm^{-1}, $\theta = -2.53$, $g = 2.08$, and $\rho = 1.13$ (%).

measured from 4 – 300 K, in equation 1, suggest weak antiferromagnetic interaction with – 2 J = 6.52 cm^{-1}. The variation of molar magnetic susceptibility, χ_m, and magnetic moment, μ_{eff}, as a function of temperature for [{Cu(HOxsbz)Cl}$_2$] is depicted in figure 8.

Different from [{Cu(Oxtsc)Cl}$_2$] where the Cu(II) centers are bridged by thiol sulfur [38], the X-ray crystal structure of [{Cu(HOxsbz)Cl}$_2$] (Section 3.4.1) reveals that the two Cu(II) ions have square pyramidal geometry and are bridged by two chlorides such that the square pyramids are arranged sharing a basal-apical edge with parallel basal planes. This type of chloride-bridged Cu(II) complex, Type II [63], is expected to show either weak antiferromagnetic or ferromagnetic behavior depending on the angle at the Cu–Cl–Cu bridge (ϕ) as well as the bond length of the longest out of plane Cu–Cl bond (R) [64, 65]. In case of **4,** the value of ϕ / R is 31.90° / Å ($\phi = 90.32^o$ and R = 2.831 Å), is lower than 32.6, which is in agreement with the observed antiferromagnetic interaction [65]. Different from [{Cu(HOxsbz)Cl}$_2$] (**4**), the Cu(II) centers in [{Cu(HOxtsc)Cl}$_2$]·H_2O are bridged by two thiolate sulfurs [38]. The different bridging modes assigned for [{Cu(HOxsbz)Cl}$_2$] (**4**) and [{Cu(HOxtsc)Cl}$_2$]·H_2O can be related to the differences in the electronic effects of the terminal – $SCH_2C_6H_5$ in **[{**Cu(HOxsbz)Cl}$_2$] as opposed to –NH_2 in [{Cu(HOxtsc)Cl}$_2$]·H_2O.

4. Conclusion

Dinuclear complexes [{Cu(Oxsbz)}$_2$]·H_2O (**1**), [{Cu(Oxtsc)}$_2$]·2H_2O (**2**), [{Cu(HOxtsc)}$_2$]$(NO_3)_2$ (**3**), [{Cu(HOxsbz)Cl}$_2$] (**4**), [{Ni(Oxsbz)}$_2$] (**5**), and [{Ni(Oxtsc)}$_2$] (**6**) as well as the mononuclear mixed ligand Ni(II) complexes [Ni(Oxtsc)HIm] (**7**) and [Ni(Oxtsc)HPyr] (**8**) have been prepared and characterized by elemental analysis and spectroscopic techniques (IR, UV–vis, ^{1}H NMR, and ESI mass). Variable temperature magnetic susceptibility measurements for [{Cu(Oxsbz)}$_2$]·H_2O, [{Cu(Oxtsc)}$_2$]·2H_2O, and [{Cu(HOxtsc)}$_2$]$(NO_3)_2$ revealed strong antiferromagnetic behavior. The -2 J values (650–690 cm^{-1}) are within the range reported for other oximate-bridged dicopper complexes. The dinuclear [{Cu(HOxsbz)Cl}$_2$], however, showed weak antiferromagnetic behavior (− 2 J = 6.52 cm^{-1}) suggesting a dichloro-bridged dicopper complex. Single-crystal X-ray diffraction of [{Cu(HOxsbz)Cl}$_2$] confirmed the dimeric structure where each Cu(II) is in square pyramidal environment and the two Cu(II) centers are linked by two chloride bridges. This bridging mode differs from that reported for the analogous thiosemicarbazone oxime complex [{Cu(HOxtsc)Cl}$_2$]·2H_2O where the Cu(II) centers are connected by thiolate rather than chloride bridges. X-ray diffraction studies on both [Ni(Oxtsc)HIm] and [Ni(Oxtsc)HPyr] showed that the central Ni(II) is in a distorted square planar environment, bound to Oxtsc dianion via the deprotonated oxime nitrogen, imine nitrogen, and deprotonated thiol sulfur. The fourth coordination site is occupied by the heterocyclic nitrogen.

Acknowledgments

The author would like to thank Sabina Foro for collecting X-ray crystal data.

Disclosure statement

No potential conflict of interest was reported by the authors.

Supplementary data

CCDC 999,736, 999,674 and 999,675 contain the supplementary crystallographic data for [{Cu(HOxsbz)Cl}$_2$], [Ni(Oxtsc)HIm], and [Ni(Oxtsc)HPyr], respectively. These data can be obtained free of charge via http://www.ccdc.cam.ac.uk/conts/retrieving.html, or from the Cambridge Crystallographic Data Center, 12 Union Road, Cambridge CB2 1EZ, UK; Fax: (+44) 1223–336-033; or E-mail: deposit@ccdc.cam.ac.uk.

References

[1] Y. Song, X.-T. Chen, C.-G. Zheng, D.-R. Zhu, X.-Z. You, L.-H. Weng. *Transition Met. Chem.*, **26**, 247 (2001).
[2] K. Matsumoto, S. Ooi, W. Mori, Y. Nakao. *J. Chem. Soc., Dalton Trans.*, 3117 (1990).
[3] R.J. Butcher, C.J. O'Connor, E. Sinn. *Inorg. Chem.*, **18**, 1913 (1979).
[4] J.A. Bertrand, J.H. Smith, D.G. VanDerveer. *Inorg. Chem.*, **16**, 1477 (1977).
[5] M. Sutradhar, T.R. Roy Barman, J. Klanke, M.C.B. Drew, E. Rentschler. *Polyhedron*, **53**, 48 (2013).
[6] J.A. Bertrand, J.H. Smith, P.G. Eller. *Inorg. Chem.*, **13**, 1649 (1974).
[7] N.M.H. Salem, L. El Sayed, S. Foro, W. Haase, M.F. Iskander. *Polyhedron*, **26**, 4161 (2007).
[8] N.M.H. Salem, L. Sayed, W. Haase, M.F. Iskander. *J. Coord. Chem.*, **58**, 1327 (2005).
[9] M.F. Iskander, L. El Sayed, N.M.H. Salem, R. Werner, W. Haase. *J. Coord. Chem.*, **56**, 1075 (2003).
[10] S.K. Chattopadhyay, D. Chattopadhyay, T. Banerjee, R. Kuroda, S. Ghosh. *Polyhedron*, **16**, 1925 (1997).
[11] N.M.H. Salem, L. El Sayed, M.F. Iskander. *Polyhedron*, **27**, 3215 (2008).
[12] A. Chakravorty. *Coord. Chem. Rev.*, **13**, 1 (1974).
[13] J.G. Mohanty, R.P. Singh, A. Chakravorty. *Inorg. Chem.*, **14**, 2178 (1975).
[14] J.G. Mohanty, A. Chakravorty. *Inorg. Chem.*, **15**, 2912 (1976).
[15] J. Korvenranta, H. Saarinen, M. Nasakkala. *Inorg. Chem.*, **21**, 4296 (1982).
[16] A.G. Lappin, M.C.M. Laranjeira, R.D. Peacock. *Inorg. Chem.*, **22**, 1983 (1983).
[17] Z.P. Deng, S. Gao, L.H. Huo, H. Zhao. *Acta Cryst.*, **E61**, m2214 (2005).
[18] V.Y. Kukushkin, D. Tudela, A.J.L. Pombeiro. *Coord. Chem. Rev.*, **156**, 333 (1996).
[19] E.S. Koumousi, C.P. Raptopoulou, S.P. Perlepes, A. Escuer, T.C. Stamatatos. *Polyhedron*, **29**, 204 (2010).
[20] A. Escuer, B. Cordero, M. Font-Bardia. *Inorg. Chem.*, **49**, 9752 (2010).
[21] M. Maekawa, S. Kitagawa, Y. Nakao, S. Sakamoto, A. Yatani, W. Mori, S. Kashino, M. Munakata. *Inorg. Chim. Acta*, **293**, 20 (1999).
[22] J.M. Dominguez-Vera, E. Colacio, A. Escuer, M. Klinga, R. Kivekäsc, A. Romerosa. *Polyhedron*, **16**, 281 (1997).
[23] A. Escuer, G. Vlahopoulou, S.P. Perlepes, F.A. Mautner. *Inorg. Chem.*, **50**, 2468 (2011).
[24] C.J. Milios, ThC Stamatatos, S.P. Perlepes. *Polyhedron*, **25**, 134 (2006).
[25] C.J. Milios, C.P. Raptopoulou, A. Terzis, F. Lloret, R. Vicente, S.P. Perlepes, A. Escuer. *Angew. Chem. Int. Ed.*, **43**, 210 (2004).
[26] P. Chaudhuri. *Coord. Chem. Rev.*, **243**, 153 (2003).
[27] C.J. Milios, S. Piligkos, E.K. Brechin. *Dalton Trans.*, 1809 (2008).
[28] S. Khanara, T. Weyhemuller, P. Chaudhuri. *Dalton Trans.*, 4675 (2007).
[29] T.S. Lobana, R. Sharma, G. Bawa, S. Khanna. *Coord. Chem. Rev.*, **253**, 977 (2009).
[30] J.S. Casas, M.S. García-Tasende. *J. Sordo. Coord. Chem. Rev.*, **209**, 197 (2000).
[31] S. Padhyé, G.B. Kauffman. *Coord. Chem. Rev.*, **63**, 127 (1985).
[32] M.J.M. Campbell. *Coord. Chem. Rev.*, **15**, 279 (1975).
[33] (a) A.V. Ablov, N.V. Gerbeleu, N.Y. Negyatse, M.D. Revenko. *Russ. J. Inorg. Chem.*, **15**, 63 (1970); (b) A.V. Ablov, N.V. Gerbeleu. *Russ. J. Inorg. Chem.*, **15**, 952 (1970).
[34] (a) R. Chikate, P.B. Sonawane, A. Kumbhar, S. Padhye, R.J. Butcher. *Inorg. Chim. Acta*, **205**, 59 (1993).; (b) P.B. Sonawane, R. Chikate, A. Kumbhar, S. Padhye. *Polyhedron*, **13**, 395 (1994); (c) P.B. Sonawane, A. Kumbhar, S. Padhye, R.J. Butcher. *Transition Met. Chem.*, **19**, 277 (1994).
[35] (a) E.A. Enyedy, E. Zsigo, N.V. Nagy, C.R. Kowol, A. Roller, B.K. Keppler, T. Kiss. *Eur. J. Inorg. Chem.*, 4036 (2012); (b) P. Souza, A.I. Matesanz, V. Fernandez. *J. Chem. Soc., Dalton Trans.*, 3011 (1996); (c) M.D. Timken, S.R. Wilson, D.N. Hendrickson. *Inorg. Chem.*, **24**, 3450 (1985).
[36] M.A. Ali, A.H. Mirza, R.J. Butcher, P.V. Bernhardt, M.R. Karim. *Polyhedron*, **30**, 1478 (2011).
[37] M.A. Ali, A.H. Mirza, L.K. Wei, P.V. Bernhardt, O. Atchade, X. Song, G. Eng, L. May. *J. Coord. Chem.*, **63**, 1194 (2010).
[38] S. Naskar, S. Naskar, H. Mayer-Figge, W.S. Sheldrick, M. Corbella, J. Tercero, S.K. Chattopadhyay. *Polyhedron*, **35**, 77 (2012).
[39] K.-Y. Choi, S.-M. Yang, K.-C. Lee, H. Ryu, C.H. Lee, J. Seo, M. Suh. *Transition Met. Chem.*, **33**, 99 (2008).
[40] A.K. Das, S. Seth, S.K. Chattopadhyay. *Z. Kristallogr.*, **215**, 481 (2000).
[41] S.K. Chattopadhyay, D. Chattopadhyay, T. Banerjee, R. Kuroda, S. Ghosh. *Polyhedron*, **16**, 1925 (1997).

[42] K.V. Katti, P.R. Singh, C.L. Barness. *J. Chem. Soc., Dalton Trans.*, 2153 (1993).
[43] A.H. Al-Kubaisi. *Bull. Korean Chem. Soc.*, **25**, 37 (2004).
[44] R. Raina, T.S. Srivastava, S. Joglekar, S.N. Shringi. *Inorg. Chim. Acta*, **76**, L197 (1983).
[45] A.V. Ablov, N.I. Belichuk, O.A. Bologa. *Russ. J. Inorg. Chem.*, **19**, 1515 (1974).
[46] Sheffield Chemputer, Isotope pattern. Available online at: http://winter.group.shef.ac.uk/chemputer/isotopes.html.
[47] (a) L. Waltz, H. Paulus, W. Haase. *J. Chem. Soc., Dalton Trans.*, 913 (1985); (b) S. Gehring, P. Fleichhauer, H. Paulus, W. Haase. *Inorg. Chem.*, **32**, 54 (1993).
[48] G.M. Sheldrick. *SHELXL-97, Shelex-97: Program for Crystal Structure Analysis*, University of Gottingen, Gottengen (1998).
[49] C.K. Johnson, M.N. Burnett. *ORTEPIII, Report ORNL-6895*, Oak Ridge National Laboratory, Oak Ridge (1996).
[50] A.L. Spek. *PLATON, A Multipurpose Crystallographic Tool*, Utrecht University, Utrecht (2002).
[51] C.F. Macrae, I.J. Bruno, J.A. Chisholm, P.R. Edgington, P. McCabe, E. Pidcock, L. Rodriguez-Monge, R. Taylor, J. van de Streek, P.A. Wood. *J. Appl. Crystallogr*, **41**, 466 (2008).
[52] K. Nakamoto. *Infrared and Raman Spectra of Inorganic and Coordination Compounds*, 4th Edn, Wiley, New York, NY (1986).
[53] M.H.S.A. Hamid, M.A. Ali, A.H. Mirza, P.V. Bernhardt, B. Moubaraki, K.S. Murray. *Inorg. Chim. Acta*, **363**, 3643 (2009).
[54] J. Garcia-Tojal, M.K. Urtiaga, R. Cortes, L. Lezama, M.I. Arriortua, T. Rajo. *J. Chem. Soc., Dalton Trans.*, 2233 (1994).
[55] E.W. Ainscough, E.N. Baker, A.M. Brodie, R.J. Cresswell, J.D. Ranford, J.M. Waters. *Inorg. Chim. Acta*, **172**, 185 (1990).
[56] A.B.P. Lever. *Inorganic Electronic Spectroscopy*, 2nd Edn, Elsevier, Amsterdam (1984).
[57] A.W. Addison, T. Nageswara Rao, J. Reedijk, J. Van Rijn, G.C. Verschoor. *J. Chem. Soc., Dalton Trans.*, 1349 (1984).
[58] M.C. Etter. *Acc. Chem. Res.*, **23**, 120 (1990).; J. Bernstein, R.E. Davis, L. Shimoni, N.-L. Chang. *Angew. Chem. Int. Ed. Engl.*, **34**, 1555 (1995).
[59] (a) M. Nishio, M. Hirota, Y. Umezaw. *The CH/π interaction, Evidence, Nature and Consequences*, Wiley, New York, NY (1998); (b) G.R. Desiraju, T. Steiner. *The Weak Hydrogen Bonds in Structural Chemistry and Biology*, Oxford University Press, Chichester (1999).
[60] Z.D. Tomic, S.B. Novakovic, S.D. Zaric. *Eur. J. Inorg. Chem.*, 2215 (2004).
[61] J.B. Hathaway, In *Comprehensive Coordination Chemistry*, G. Wilkinson, R.D. Gillard, J.A. McCleverty (Eds.), Vol. 5, Pergamon Press, New York, NY (1987).
[62] O. Kahn. *Molecular Magnetism*, Wiley–VCH, New York (1993).
[63] M. Rodríguez, A. Llobet, M. Corbella, A.E. Martell. *Inorg. Chem.*, **38**, 2328 (1999).
[64] W.E. Marsh, K.C. Patel, W.E. Hatfield, D.J. Hodgson. *Inorg. Chem.*, **22**, 511 (1983).
[65] W.A. Alves, R.H. de Almeida Santos, A. Paduan-Filho, C.C. Becerra, A.M. Da Costa Ferreira. *Inorg. Chim. Acta*, **357**, 2269 (2004).